ICAS-88-4.2.3

EFFICIENT NUMERICAL SIMULATION OF TURBULENT FLOWS

E. Arad† and M. Wolfshtein‡
†ADA - Armament Development Authority, Ministry of Defense, Israel
‡Technion - Israel Institute of Technology

Abstract

The paper describes an efficient solver for two dimensional turbulent boundary layers based on OCI techniques. The boundary conditions are given in a general problem independent way. The method is applicable to any two equation turbulence model. The application of the method to two equations turbulence models is discussed. A rational way to utilize the method for optimization of two equation turbulence models is presented. Sample results are shown.

1. Introduction

1.1 The Problem Considered

This paper is concerned with the calculation of turbulent boundary layers using a two equation model of turbulence. The numerical solution of this problem is difficult due to two reasons. Firstly the second model equation, representing the scale of the turbulence is difficult to model. This is a difficulty with any scale equation, be it the popular dissipation equation, or any other second model equation. Secondly, the distribution of the velocity, turbulent energy and turbulent scale is not very regular. Each of the variables has steep gradients in a different part of the field. Thus a fine mesh is required in most of the field, which is expensive to compute. These two difficulties make the numerical modeling of turbulent boundary layers a demanding and uneasy task.

The aim of the present research is to study an optimal scale equation for two equation turbulence models. The optimization should be done by comparison of experimental and computed results for many cases. In order to do this it was necessary to develop efficient boundary layer solver. Therefore the research is concerned with two topics: (i) efficient method for the numerical solution of turbulent boundary layer equations; (ii) optimization of the second model equation utilizing the efficient scheme to be developed according to (i) above. In this paper the general strategy is discussed and the special efficient numerical methods developed for the project are presented.

1.2 Literature Survey

The closure problem of turbulent flows is well known for a long time. Various answers to the problem have been proposed, ranging from the simple integral methods, to the direct simulation using super computers, as was demonstrated in the Stanford 1982 conference on complex turbulent flows [1]. Typically these two extreme cases offer very distinct advantages. The simple integral methods as well as the mixing length models offer fast and cheap means for the calculations. Moreover they work very well for a surprisingly large number of cases. Yet there are cases of practical significance in which these methods can not offer an acceptable solution. In the other extreme of direct simulation the quality of the results is very good if the Reynolds number is not too high and the mesh is sufficiently fine. Yet the price of the computation is immense. Thus it becomes necessary to employ higher order turbulence models for many practical applications. Various modeling options have been studied, but the two equation turbulence models are without any doubt the most acceptable choice due to their relative simplicity and ease of computation.

Two equation models are based on the eddy viscosity hypotheses. In this sense they share some weakness with the simpler mixing length model. They differ from the mixing length model by relating the eddy viscosity to the amplitude and frequency of the turbulent velocity fluctuations, obtained by a solution of two partial differential equations. Thus they can predict cases in which the history of the turbulence is important at the price of heavier needs for computer resources.

The amplitude of the velocity fluctuations is usually related to the turbulence energy. The frequency is obtained from the scale of the turbulence as well as the turbulence energy itself. The standard practice today is to use the dissipation equation as formulated by Jones and Launder [2] as the standard second model equation. The energy-dissipation model was discussed in some detail in the 1982 Stanford Conference on complex turbulent flows [1]. The evaluation committee of this conference wrote: "The weakest point of present one-point closure is the epsilon equation. The computed results of many flows can be brought into good agreement with the data by tweaking the epsilon equation constants. A better equation should make these changes in value an automatic part of the calculation. A corollary effect of the epsilon equation defects is the too large length scale in adverse pressure gradients and near separation." This conclusion was substantiated by Mansour et. al. [3] who found large discrepancies between the modeled term of the dissipation equation and the ones computed using direct simulations.

With this remark in mind it seems appropriate to seek alternative formulation for the second model equation. Of course the dissipation equation has been used for this purpose for a very long time. Wilcox and Rubesin [4] has used an energy-vorticity model, while and Arad et. al. [5] used an energy-length scale model. It was found that these models may produce results which are of the same quality as the dissipation model, but they are more cumbersome. Other models were proposed by Lin and Wolfshtein [6] for a "volume of turbulence" and by Zeierman and Wolfshtein [7] for a "time scale of turbulence". These models were not seriously tried in numerical simulations.

Numerical solutions of the turbulence models equations are performed often these days. However, such solutions are not simple and require considerable computer

time. The problem becomes much easier when boundary layers are considered, and the character of the governing equations change from elliptic to parabolic. A major problem in the numerical solution of boundary layer problems is the growth of the boundary layer thickness, requiring an expanding mesh along the flow direction. Two approaches are possible here: Either to widen the mesh using a given formula for the boundary layer thickness (e.g. Pade et. al. [8]), or to use some approximate method for the calculation of the boundary layer thickness any time a new step is performed (e.g. Patankar and Spalding [9]).

The CPU time requirements for a given (high) accuracy may be reduced by using a high order numerical scheme. Yet, high order schemes may impose stability, algorithmic and programming problems. Thus Patankar and Spalding [9] preferred a first order scheme to avoid stability problems. Cebeci and Smith [10] used the second order Keller box scheme [11] as a means to get an efficient solver. Arad et. al. [5] found that even a second order accuracy requires many mesh points for a solution of boundary layers with a two equation turbulence model, due to the steep gradients of different variables in different parts of the flow field. Postan et. al. [12] report similar conclusions for flows with high pressure gradients and concluded that a fourth order scheme is to be preferred.

High order finite difference schemes of various kinds have been reported in the literature. Of the many possibilities we prefer in this work those which retain the tridiagonal nature of the matrices, and do not require solution of auxiliary differential equations. This preference leads to the choice of "Operator Compact Implicit" fourth order schemes proposed by Swartz [13].

The application of the OCI scheme to boundary layer problems is usually done by approximating the lateral part of the differential operator by high order scheme. The methods reduce to tri—diagonal form. Ciment, Leventhal and Weinberg [14] applied this approach to the solution of parabolic equations.

The stability characteristics of the OCI scheme are of serious concern. Berger, Solomon, Ciment, Leventhal and Weinberg [15] who used the OCI schemes for the solution of the boundary layer equations treated the problem of limiting stability requirements, originating from the small value of the diffusion coefficient ϵ, typical to high Reynolds number problems. Similar boundary layer equations, with strong pressure gradients, were solved using the OCI scheme by Postan et. al. [12].

Another way to reduce the computational load is to use wall functions, as suggested by Patankar and Spalding [9]. Arad and Wolfshtein [16] showed that in certain cases the use of wall functions may bring a dramatic reduction in the number of mesh points required for a given accuracy. Yet, the application of wall functions requires very good one dimensional solutions for the region very near to the wall. This is not an easy task for the turbulence model equations.

1.3 Definition of The Problem

In view of the above, the aims of the paper are to describe an efficient method for the solution of boundary layer problems and its application to turbulence modeling. The problems of wall functions, boundary layer thickness adaptive grids and mesh stretching are addressed as well. The application of the method to the optimization of two equation turbulence modeling is discussed, and the associated mathematical problem is described.

2. Two Equations Turbulence Models

Two equation turbulence models are based on the assumption that turbulence may be described by two variables representing the amplitude and frequency of the turbulent fluctuations. In most models ever used the amplitude is represented by the turbulence kinetic energy defined by

$$e \equiv \overline{u_i' u_i'} \tag{2.1}$$

The second variable may be viewed as a product of the energy and the scale raised to some power. The variables considered in this work are the dissipation (ϵ), the length scale of turbulence (l), the volume of turbulence (V), the time scale of turbulence (T) and a generalized variable (ϕ). We define the generalized scale ϕ by

$$L = C_L e^{\alpha} \phi^{\beta} \tag{2.2}$$

where C_L is an empirical coefficient and ϕ may stand not only for the generalized variable but also for any of the explicit scale variables. The values of the constants α and β for the four models considered here are:

ϕ	$e-\epsilon$	$e-L$	$e-V_{ij}$	$e-T$
α	1.5	-1	$-\frac{1}{2}$	$-\frac{1}{2}$
β	-1	1	$\frac{1}{3}$	1

The energy-dissipation turbulence model is undoubtedly the model used for the large majority of computations nowadays. However, it is easy to derive the governing equations for the other variables from the dissipation equation, and it is possible to make all such models fully identical in the sense that they will yield exactly the same eddy viscosity. It should be noted that this is not the way these equations are usually derived: In most cases some physical meaning is assigned to the scale variable, and a corresponding mathematical definition is applied. The result of modeling the exact equations obtained in this way is very similar to that obtained when the equation for the variable is derived from the dissipation equation. The differences are almost always confined to the source term of the equation as is shown below.

The governing equations for both the turbulent energy and the scale always have the following form:
convection = diffusion + production - decay + source.
Thus the conservation equation for the turbulent energy is:

$$\rho \frac{De}{Dt} = \frac{\partial}{\partial y}\left[\left(\mu + \frac{\mu_t}{\sigma_e}\right)\frac{\partial e}{\partial y}\right] + \mu_t \left(\frac{\partial U}{\partial y}\right)^2 - \rho D_e \tag{2.3}$$

where $D_e = \epsilon$ is the turbulent energy dissipation.
The conservation equation for the generalized scale, ϕ is:

$$\frac{D\phi}{Dt} = T_\phi + P_\phi - D_\phi + S_\phi \tag{2.4}$$

It is common to treat the diffusion term T_ϕ as gradient dependent:

$$T_\phi = \frac{\partial}{\partial x_i}\left[\left(\mu + \frac{\mu_t}{\sigma_\phi}\right)\frac{\partial \phi}{\partial x_i}\right] \tag{2.5}$$

where σ_ϕ is the empirical turbulent Prandtl number for ϕ. The production term P_ϕ is formulated using the production term in the turbulence energy equation (P_e):

$$P_\phi = C_g \frac{\phi}{e} P_e \tag{2.6}$$

In the same manner, the decay term D_ϕ is:

$$D_\phi = C_d \frac{\phi}{e} D_e \tag{2.7}$$

The turbulent viscosity is calculated by the following formula:

$$\mu_t = C_\mu C_L e^{\alpha+\frac{1}{2}} \phi^\beta \tag{2.8}$$

Seven empirical coefficients are used, namely:
$C_g, C_1, C_L, C_d, C_\mu, \sigma_e, \sigma_\phi$. The length scale has a physical meaning and significance. However, it is often the case that in the calculations we wish to predict correctly only the eddy viscosity, and not the length scale, or its representative variable ϕ. In this case C_L may be taken as unity without any loss of generality and either C_μ or C_1 can be fixed arbitrarily as well, thus reducing the number of empirical coefficients to 5.

The list of these coefficients is written below:

ϕ	$e-\epsilon$	$e-L$	$e-V_{ij}$	$e-T$
C_1	1.	0.09		1.
C_g	1.44	0.98		0.173
C_d	1.92	0.055		1.
C_μ	0.09	1.		0.09
σ_e	1.	1.		1.46
σ_ϕ	1.3	1.		10.8

The coefficients of the energy-volume model are not known at the present time. The energy-length model has the following source term:

$$S_L = -\left(C_4 \frac{L}{y}\right)^q \cdot eLP_e \tag{2.9}$$

$$C_4 = 8.83 \qquad q = 6$$

Computational experience suggests that the energy dissipation model does not usually require a source term in the dissipation equation.

We wish to emphasize that all models can be brought into a generalized form. In this form the coefficients related to the generation and dissipation are about the same in all models, and the corresponding terms are exact transformations of one another. The main difference between the models is in the diffusion terms. Transformation of these terms from one model to the other always leaves a residual term which must be added to the source term. The residual source term created by transforming the diffusion term of the energy-dissipation equation to the generalized formulation is:

$$\begin{aligned} S_\phi = & \\ & \frac{\partial}{\partial x_j}\left[\mu_t\left(\frac{1}{\sigma_\epsilon}-\frac{1}{\sigma_\phi}\right)\frac{\partial \phi}{\partial x_j}\right] + \\ & + \frac{3/2-\alpha}{\beta}\left(\frac{1}{\sigma_e}-\frac{1}{\sigma_\phi}\right)\frac{\phi}{e}\frac{\partial}{\partial x_j}\left(\mu_t \frac{\partial e}{\partial x_j}\right) - \\ & - \frac{3/2-\alpha}{\beta}\frac{\phi}{e^2}\left(\mu+\frac{\mu_t}{\sigma_e}\right)\left(\frac{\partial e}{\partial x_j}\right)^2 - \\ & - \frac{\beta+1}{\phi}\left(\mu+\frac{\mu_t}{\sigma_\epsilon}\right)\left(\frac{\partial \phi}{\partial x_j}\right)^2 + \\ & + 2\frac{3/2-\alpha}{\beta}\left(\mu+\frac{\mu_t}{\sigma_\epsilon}\right)\frac{\partial e}{\partial x_j}\frac{\partial \phi}{\partial x_j} \end{aligned} \tag{2.10}$$

The two leading terms have the form of diffusion terms for e and ϕ. The second part has the following form:

$$a_1\left(\frac{\partial e}{\partial x_j}\right)^2 + a_2\left(\frac{\partial \phi}{\partial x_j}\right)^2 + a_3\left(\frac{\partial e}{\partial x_j}\frac{\partial \phi}{\partial x_j}\right) \tag{2.11}$$

An optimal two-equation model may be defined as one which gives best agreement with experimental data while still requiring no source term, or at least the simplest sources term. This optimal model is not necessarily any of the four models presented above. The optimal model may be defined as this model which uses such a combination of α and β, which satisfies the optimization demands.

The most important feature of an optimal model is the capability to handle a large range of physical cases. Variables which can be directly measured are superior, since the model results can be easily validated by experiments. Comparisons with full simulation, may yield better understanding as well. As shown, the source terms often contain mixed terms (from both the energy and scale equations). It is therefore always advantageous to use a model with smaller source term thus reducing the coupling between the equations.

3. Mathematical Presentation

3.1 Formulation

A detailed formulation of the problem is given by Arad et. al. [5]. Thus, only a brief summery is presented here. The conservation equations of mass, momentum and energy, for a steady boundary layer are:

$$\frac{\partial \rho u r}{\partial x} + \frac{\partial \rho v r}{\partial y} = 0$$

$$\rho u \frac{\partial u}{\partial x} + \rho v \frac{\partial u}{\partial y} = -\frac{dP}{dx} + \frac{1}{r}\frac{\partial}{\partial y}\left(\mu_{eff} r \frac{\partial u}{\partial y}\right) \tag{3.1.1}$$

$$\begin{aligned} & \rho u \frac{\partial h_0}{\partial x} + \rho v \frac{\partial h_0}{\partial y} = \\ & = \frac{1}{r}\frac{\partial}{\partial y}\left\{r\left[\frac{\mu_{eff}}{\sigma_h}\frac{\partial h_0}{\partial y} + \left(1-\frac{1}{\sigma_h}\right)\mu_{eff}\frac{\partial}{\partial y}\left(\frac{u^2}{2}\right)\right]\right\} \end{aligned}$$

The unknowns in these equations are the velocity components u and v, and the stagnation enthalpy h_0. The effective viscosity is defined by:

$$\mu_{eff} = \mu + \mu_t \tag{3.1.2}$$

The turbulent viscosity (μ_t) is calculated by a turbulence model.

One of the boundaries for the problem is a solid wall with no-slip boundary conditions. The second boundary is usually the main stream which is governed by the potential flow equations. Specification of the no slip boundary conditions on the wall requires a solution right through the viscous sublayer and up to the wall. This procedure requires fine grids to handle the strong gradient near the wall. Moreover, a set of viscous damping functions is required in order to represent the viscous sublayer well. It is difficult to devise such functions in a universal way. The other possibility is to use wall functions, thus eliminating the need to solve up to the wall. The universality of the wall functions is similar to that of the damping functions mentioned above.

When the solution is carried out up to the wall, the velocity, the turbulence energy and the length scale of turbulence are zero on the inner boundary. The implications to various models have to be worked out. For the enthalpy, two boundary conditions are possible: Either a given heat flux or a given temperature.

When wall functions are used the computational boundary is removed from the solid wall. The distance between the two, y_b, should satisfy the following condition:

$$30 \le y_b^+ \le 150 \tag{3.1.3}$$

where

$$y_b^+ = \frac{\rho u_\tau y_b}{\mu} \tag{3.1.4}$$

u_τ is the friction velocity. The "universal law of the wall", determines boundary conditions for the momentum equation. For computational reasons it is easier to use the power law approximation for the law of the wall:

$$\begin{aligned} \frac{u}{u_\tau} &= a\left(\frac{y u_\tau}{\nu}\right)^{1/n} \\ \frac{\partial u}{\partial y} &= \frac{u}{ny} \end{aligned} \tag{3.1.5}$$

where

$$\begin{aligned} n &= log\,(EY_+) \\ a &= \frac{n}{\kappa} Y_+^{-\frac{1}{n}} \end{aligned} \tag{3.1.6}$$

E=9, $\kappa = 0.41$ (Von-Karman constant). Experimental data suggests that the boundary condition for the the turbulence energy, e, is given by:

$$\frac{e}{u_\tau^2} = \frac{10}{3} \tag{3.1.7}$$

Assuming a balance of generation and decay (e.g. when the convection and diffusion are negligible) in the universal wall region, the following condition is obtained for ϕ:

$$\frac{\phi^\beta e^\alpha}{y} = \sqrt{\frac{C_1}{C_\mu}} \frac{\kappa}{C_L} \frac{e^{1/2}}{u_\tau} \tag{3.1.8}$$

On the main stream boundary the velocity and enthalpy are determined by the external solution, which is usually potential and isentropic. The turbulent quantities may be calculated there by neglecting the turbulence generation and diffusion, yielding equations for the other variables:

$$\begin{aligned} \frac{DU_i}{Dt} &= -\frac{\partial P}{\partial x_i} \\ \frac{De}{Dt} &= -D_e \\ \frac{D\phi}{Dt} &= -D_\phi \end{aligned} \tag{3.1.9}$$

3.2 Transformations

The coordinates transformations used in the present work are designed to allow the mesh to expand with the boundary layer thickness and to concentrate more mesh points near the solid wall, where the gradients are steepest. The first goal is obtained by transformation to the Patankar and Spalding normalized stream function coordinates [9].

$$\omega = \frac{\psi}{\psi_E - \psi_I} \tag{3.2.1}$$

where

$$\psi = \left[\int_0^Y (\rho u r)\, dy\right]_{x=const.} \tag{3.2.2}$$

and ψ_E and ψ_I are the stream function values on the external and internal boundaries, respectively. In this co-ordinate system, the continuity equation is satisfied automatically due to the use of the stream function co-ordinates. Moreover, the grid is self-adaptive to the thickness of the boundary layer. Arad et. al. [5] showed, that in this co-ordinate system, the cross-flow derivative of velocity is singular near the wall. This singularity was removed using a square root transformation to the (x,z) plane,where

$$z = \omega^{1/2} \tag{3.2.3}$$

Under this transformation, an equation for a general variable F can be written, as follows:

$$\frac{\partial \mathbf{F}}{\partial x} + \frac{b}{2z}\frac{\partial \mathbf{F}}{\partial z} = \frac{1}{2z}\frac{\partial}{\partial z}\left(C\frac{\partial \mathbf{F}}{\partial z}\right) + d \tag{3.2.4}$$

The general variable F represents the velocity, total enthalpy and the variables of the turbulent model (turbulence energy and scale, in the present case). The equation coefficients for these variables are the following:

$$b = \frac{r_E \dot{m}''_E}{\Psi_E} \quad C = \frac{r^2 \rho \Gamma u}{2z\Psi_E^2} \quad \Gamma = \mu_L + \frac{\mu_t}{\sigma_F} \tag{3.2.5}$$

The source term is split into two parts:

$$d_i = s_{i,U} + s_{i,D}\mathbf{F}_{i,D} \tag{3.2.6}$$

Thus the the source is given by:

$$S_{i,U} = \begin{cases} -\frac{1}{\rho u}\frac{dP}{dx} \\ \frac{\partial}{\partial y}\left[\left(1-\frac{1}{\sigma_h}\right)\right. \\ \left.\frac{\mu_{eff}}{\rho u}\frac{\partial}{\partial y}\left(\frac{u^2}{2}\right)\right] \\ \frac{\mu_t}{\rho u}\left(\frac{\partial U}{\partial y}\right)^2 \\ \left(c_2 f_2 - \frac{F_4}{f_4}\right)\frac{l\mu_t}{\rho u}\left(\frac{\partial U}{\partial y}\right)^2 \end{cases} \qquad S_{i,D} = \begin{cases} 0 \\ 0 \\ -\frac{c_1}{f_1}\frac{e^{1/2}}{lu} \\ -\frac{c_3}{f_3}\frac{e^{1/2}}{ul} \end{cases}$$

For stability reasons, it is preferable to make the explicit part (S_U) as small as possible.
The former transformation is sufficient for obtaining laminar flow solutions. Yet the strong gradients which characterize the turbulent regime require a finer mesh in the wall vicinity. Such a refinement may be obtained using logarithmic transformation:

$$\varsigma = \frac{ln\left(1.+\frac{z-z_0}{\beta}\right)}{ln\left(1.+\frac{1-z_0}{\beta}\right)} \qquad (3.2.7)$$

For small β, a very dense mesh is created near the wall. An equivalent stretching is obtained by Arad et al. [5], using an arc-tangent function. Here the lower boundary is z_0, which is not necessarily zero (as in the case of wall functions). This clustering transformation is sufficient for wall function version. Yet, when solution up to the wall was performed, the strong clustering which is required near the wall results in a very poor resolution in the external regions of the boundary layer, and large errors in the integral coefficients. The problem becomes significant in the coarse grids which are used for the fourth order solution, and is negligible in the fine grids which are required for the second order solutions. Pade et. al. [8] proposed a two layer transformation, to overcome this difficulty: The inner region of the boundary layer is mapped by a fourth order polinom, while the external part is mapped by a power low transformation:

$$\varsigma = \begin{cases} Az + Bz^2 + Cz^3 + Dz^4 & for \quad \varsigma \leq \varsigma_m \\ z^\alpha & for \quad \varsigma \geq \varsigma_m \end{cases} \qquad (3.2.8)$$

In the matching point, continuity of the derivatives up to the second order is maintained. Allowing a slight discontinuity in the third derivative releases another degree of freedom in the grid control, without any problem in the solution of a second order equation.

3.3 Boundary Layer Thickness and Entrainment

The boundary layer thickness, δ, does not have a significant importance in this formulation of the boundary layer problem. It is needed only for the coordinate transformation and for calculating the marching step (Δx). Following this philosophy Patankar and Spalding [1] and Arad et. al. [5] estimated the boundary layer thickness from the entrainment, e.g. $\frac{\partial \Psi_E}{\partial x}$ for each step in the marching direction. The entrainment was calculated using a reduced approximate form of the momentum equation on the external boundary. The justification for this formulation, presented in ref. [9], is rather frail, particularly in the laminar case where the external boundary is not definite. Moreover, the entrainment, and hence the boundary layer thickness, appear to be dependent on the lateral step size Δy near the external boundary, which have no physical meaning. As a result, the boundary layer thickness depends on the number of points in the lateral direction.

All this is acceptable in a second order solution with many mesh points as the solution does not really depend on δ. The friction coefficient as well as the displacement and momentum thicknesses, are not affected by the error in estimating the boundary layer thickness. However, when a fourth order method is used with coarse grid, large errors occur in all these quantities. Therefore a better approximation of the boundary layer thickness is required. This was achieved by using the boundary layer integral momentum equation:

$$\frac{d\Theta}{dx} + \frac{\Theta}{U_\infty}\frac{dU_\infty}{dx}\left(2 + H - M_\infty^2\right) = \frac{1}{2}C_f \qquad (3.3.1)$$

The values of the shape factor, H, and the friction coefficient C_f can be taken from the previous step. Then equation 3.3.1 becomes an ordinary differential equation for the momentum thickness Θ with the solution:

$$\Theta_D = \begin{cases} \Theta_U + \frac{1}{2}C_f\Delta x & for \quad \frac{dU_\infty}{dx} = 0 \\ \frac{C_f}{2a} + \left(\Theta_U - \frac{C_f}{2a}\right)e^{-a\Delta x} & for \quad \frac{dU_\infty}{dx} \neq 0 \end{cases} \qquad (3.3.2)$$

$$a = \frac{1}{U_\infty}\frac{dU_\infty}{dx}\left(2 + H - M_\infty^2\right)$$

Using the definition of the momentum thickness, the boundary layer thickness of the next step is estimated:

$$\delta^{n+1} = \frac{\Theta^{n+1}}{\left[\int_0^1 \frac{u}{U_\infty}\left(1-\frac{u}{U_\infty}\right)\right]^n d\eta} \qquad (3.3.3)$$

The entrainment which is defined as the derivative of the stream function with respect to x on the external boundary, can be calculated using the definition of the stream function:

$$\frac{d\Psi_E}{dx} = \frac{d}{dx}\int_0^\delta \rho u r dy \quad = \quad \int_0^\delta \frac{\partial(\rho r u)}{\partial x}dy + \rho_E u_E r_E \frac{d\delta}{dx} \qquad (3.3.4)$$

and the continuity equation:

$$\frac{\partial}{\partial x}(\rho u r) = -\frac{\partial}{\partial y}(\rho v r) \qquad (3.3.5)$$

Substitution of (3.3.5) in (3.3.4) yields:

$$\frac{d\Psi_E}{dx} = -\delta\rho_E v_E r_E + \rho_E r_E u_E \frac{d\delta}{dx} \qquad (3.3.6)$$

and the x derivative of δ is calculated by a forward second order scheme:

$$\frac{d\delta}{dx} = \frac{3\delta^{n+1} - 4\delta^n + \delta^{n-1}}{2\Delta x} + o\left(\Delta x^2\right) \qquad (3.3.7)$$

3.4 Wall Functions

The simplest way to use wall functions is by matching the finite difference solution with the wall functions over the two innermost points (indexed "1" and "2"). This is very simple when the power law formulation (3.1.5) is used as the boundary condition is reduced to:

$$\frac{u_2}{u_1} = \left(\frac{y_1}{y_2}\right)^{1/n} \qquad (3.4.1)$$

It is not difficult to define a two point formula using the logarithmic profile as well, but in this case the formulation is implicit and non-linear.

In two point matching the universal law of the wall must hold not only for the point y_1 but also for the point y_2. This may require a fine mesh spacing near the inner boundary.

A different possibility is to use a single point formulation. Let us consider first simple central second order approximation, using a fictitious point y_0 outside of the physical domain. We start by writing the finite difference analog of eq. (3.1.5):

$$\frac{U_2 - U_0}{2h} = \frac{U_1}{ny_1} \qquad (3.4.2)$$

Considering this equation as the one for U_0, it is not diagonally dominant, and the formulation is not stable. First order approximation of the normal derivative yields a stable formulation:

$$\left(1 + \frac{h}{ny_1}\right) U_1 - U_2 = 0 \qquad (3.4.3)$$

Arad and Wolfshtein (16) suggested an alternative approach which achieves both stability and second order accuracy. It uses the finite difference equation (4.1.2) at the boundary point y_1 together with the second order boundary condition formulation (3.4.2). In this case the variable U_0 is eliminated and the equation becomes:

$$\left(b_1 - \frac{2h}{ny_1}\right) U_1 + (a_1 + c_1) U_2 = d_1 \qquad (3.4.4)$$

3.5 Calculation of Skin Friction

When the interior boundary conditions are defined using wall functions, the "universal law of the wall" is used to calculate the skin friction. The expression is simplified using the law of the wall and its derivative with respect to the distance from the wall:

$$\begin{aligned} U &= f(y, u_\tau, \mu, \rho) \\ \frac{\partial U}{\partial y} &= g(y, u_\tau, \mu, \rho) = f' \end{aligned} \qquad (3.5.1)$$

When the logarithmic law of the wall is used the skin friction is calculated from:

$$\frac{\tau}{\rho u^2} = \frac{\kappa^2}{ln\left[E\frac{\rho u y}{\mu}\left(\frac{\tau}{\rho u^2}\right)^{1/2}\right]^2} \qquad (3.5.2)$$

Where E and κ are universal constants, and u_τ is the friction velocity. This expression is implicit, and its solution requires iterations. If Newton-Raphson iterations are used converged solution may be obtained within 2-3 iterations.

The wall functions, like the friction law which was given here, do not formally conserve the fourth order accuracy. Yet, the significant saving in computational effort which is the benefit of their use (16), makes this concept attractive. The formal fourth order accuracy may be conserved when the solution is performed up to the wall. Compact approximation was used in this case, where analytical information was used to conserve the fourth order accuracy. The first derivative was calculated using Taylor series expansion, and the higher derivatives in the series where given by the laminar, incompressible momentum equation, which is valid in the close vicinity of the wall.

4. Numerical Formulation

4.1 OCI Formulation

The numerical method used in this work belongs to the OCI family (Operator Compact Implicit). The properties of this type of numerical methods are discussed in chapter 1. The particular scheme described below is due to Israeli and Livne (17) for the solution of a partial differential equation of the following form:

$$\frac{\partial \Phi}{\partial x} = L(\Phi)$$

where

$$L(\Phi) = \frac{\partial^2 \Phi}{\partial y^2} + P(\Phi, y)\frac{\partial \Phi}{\partial y} + Q(\Phi, y)\Phi - f(y) \qquad (4.1.1)$$

If N is the number of grid points in the y direction, and the constant cell size in the transformed plane is $h = \frac{1}{N}$, then the general OCI scheme is:

$$a_j\Phi_{j-1} + b_j\Phi_j + c_j\Phi_{j+1} = \alpha_j f_{j-1} + \beta_j f_j + \gamma_j f_{j+1} \qquad (4.1.2)$$

The scheme 4.1.2 is of the $p \geq 1$ order, if for any function V

$$L_h V = LV + O\left(h^p\right) \qquad (4.1.3)$$

where L_h is a finite difference operator.
Let $V_j = y^j \quad 0 \leq j \leq 4$, then for $L_h V_j = 0$, $f(y) = j(j-1)y^{j-2} + P(y)jy^{j-1} + Q(y)y^j$. Equating $L_h V$ to zero for $0 \leq j \leq 4$, gives five linear equations, with six unknowns: a,b,c,α, β, γ: One of the constants may be arbitrarily chosen without loss of generality. If we choose β to be

$$\beta = 60 + 16h\left(P_{j+1} - P_{j-1}\right) - 4h^2 P_{j+1}P_{j-1} \qquad (4.1.4)$$

then the other coefficients are defined as follows

$$\alpha = 6 + h\left(2P_{j+1} - 5P_{j-1}\right) - h^2 P_j P_{j+1}$$
$$\gamma = 6 + h\left(5P_j - 2P_{j-1}\right) - h^2 P_j P_{j-1}$$
$$a = \frac{\alpha+\beta+\gamma}{h^2} + \frac{-3\alpha P_{j-1} - \beta P_j + \gamma P_{j+1}}{2h} + \alpha Q_{j-1}$$
$$b = -2\frac{\alpha+\beta+\gamma}{h^2} + 2\frac{\alpha P_{j-1} - \gamma P_{j+1}}{h} + \beta Q_j$$
$$c = \frac{\alpha+\beta+\gamma}{h^2} + \frac{-\alpha P_{j-1} + \beta P_j + 3\gamma P_{j+1}}{2h} + \gamma Q_{j+1} \tag{4.1.5}$$

Equation 4.1.2 is tri—diagonal and can be easily solved by a recursive algorithm, once the proper boundary conditions are introduced.

4.2 High Order Boundary Conditions

The second order differential equation requires definition of boundary conditions, on both the external and internal boundaries. The most general form of the boundary conditions is

$$\begin{aligned} W_L &= T_L\Phi_L + S_L\left(\Phi_y\right)_L \\ W_H &= T_H\Phi_H + S_H\left(\Phi_y\right)_H \end{aligned} \tag{4.2.1}$$

These expressions contain the first derivatives on the boundaries which should be approximated to at least the same order as the solver. To avoid multi—point fluctuation sensitive formulae, the derivative is discretized by the following simple Taylor expansion:

$$\Phi_y = \frac{\Phi_{j+1} - \Phi_j}{h} - \frac{h}{2}\Phi_j'' - \frac{h^2}{6}\Phi_j''' - \frac{h^3}{24}\Phi_j^{iv} + O\left(h^4\right) \tag{4.2.2}$$

The higher derivatives are evaluated using the differential equation (4.1.1). For simplicity, the method is explained for second order accuracy:

$$\Phi'' = f - P\Phi' - Q\Phi \tag{4.2.3}$$

Substituting equation 4.2.3 into equation 4.2.2, and rearranging the equation to solve for Φ', yields:

$$\left(1 - \frac{h}{2}P\right)\Phi' = \frac{1}{h}\Phi_{j+1} + \left(-\frac{1}{h} + \frac{h}{2}Q\right)\Phi - \frac{h}{2}f + O\left(h^2\right) \tag{4.2.4}$$

Differentiation of (4.2.3) results in expressions for the third and fourth order derivatives:

$$\begin{aligned} \Phi''' &= f' - P\Phi'' - \left(P' + Q\right)\Phi' - Q'\Phi \\ \Phi^{iv} &= f'' - P\Phi''' - \left(2P' + Q\right)\Phi'' - \left(P'' + 2Q'\right)\Phi' - Q''\Phi \end{aligned} \tag{4.2.5}$$

Expression 4.2.5 is substituted into 4.2.2. Solving for Φ', in the same manner used for the derivation of (4.2.3), yields fourth order formulation for the first derivative:

$$\begin{aligned} &\left\{1 - \frac{h}{2}P + \frac{h^2}{6}\left(P^2 - P' - Q\right) + \right. \\ &\left. + \frac{h^3}{24}\left[-P'' + 3PP' + P\left(2Q - P^2\right) - 2Q'\right]\right\}\Phi' = \\ &= \frac{1}{h}\Phi_{j+1} + \\ &+ \left\{\frac{-1}{h} + \frac{h}{2}Q + \frac{h^2}{6}\left(-PQ + Q'\right) + \right. \\ &\left. + \frac{h^3}{24}\left[Q'' - PQ' - Q\left(2P' - P^2 + Q\right)\right]\right\}\Phi_j + \\ &- \frac{h}{2}f + \frac{h^2}{6}\left(Pf - f'\right) + \frac{h^3}{24}\left[-f'' + Pf' - \right. \\ &\left. - f\left(P^2 - 2P' - Q\right)\right] \end{aligned} \tag{4.2.6}$$

Expression (4.2.6) is substituted into equation (4.2.1), giving the difference equations for the boundary nodes.

4.3 Application of The OCI Scheme to The Boundary Layer Equations

In chapter 3., the general conservation equation (3.2.4) was derived for a general variable F representing the velocity, total enthalpy turbulent energy and turbulent length scale. This equation is first discretized in the x direction:

$$F_x = \frac{1}{\Delta x}\left(F^{n+1} - F^n\right) \tag{4.3.1}$$

This equation has now to be recast in the form

$$F_{zz} + P(z)F_z + Q(z)F = R(z) \tag{4.3.2}$$

It is not difficult to rearrange the equation and get

$$\begin{aligned} P &= \frac{1}{C}\frac{\partial C}{\partial z} - \frac{1}{C}bz^2 \\ Q &= \frac{2z}{C}\left(-\frac{1}{\Delta x} + s_D\right) \\ R &= -\frac{2z}{\Delta x C}\Phi^n - \frac{2z}{C}s_U \end{aligned} \tag{4.3.3}$$

It should be noted that the conservation equation is not written in the conservative form any more. Furthermore, before the solution is performed, the derivative of the coefficient (C) in the diffusion term should be approximated. Evidently, this approximation should be of the fourth order, to preserve the order of the solver. The approximation of the first derivative of the diffusion term is done by an implicit compact algorithm. The method is based on the following hermit approximation due to Ciment et. al. [14]:

$$\frac{1}{6}\left[\left(U_x\right)_{j+1} + 4\left(U_x\right)_j + \left(U_x\right)_{j-1}\right] = \frac{U_{j+1} - U_{j-1}}{2h} \tag{4.3.4}$$

In principle the boundary conditions for the above system should be specified to the same order as the system. This was not the case on the exterior boundary where second order scheme was found sufficient. However, the application of a second order boundary condition on the interior boundary caused the loss of the fourth order accuracy over the entire range. A fourth order multi-point approximation of this boundary condition caused strong oscillations and loss of stability. Consequently, the boundary condition for the first derivative on the interior boundary, had to be defined analytically. Differentiation of the diffusion term (C - 3.2.5) with respect to z, while neglecting the density derivatives yields:

$$\frac{\partial C}{\partial z} = \frac{\rho r^2}{2\Psi_E^2}\left[\frac{\Gamma}{z}\frac{\partial u}{\partial z} + \frac{u}{\sigma z}\frac{\partial \mu_t}{\partial z} - \frac{\Gamma u}{z^2}\right] \tag{4.3.5}$$

The chain rule and the transformations definitions were

used to calculate the terms of (4.3.5). For the case of wall functions, the universal law of the wall was used:

$$\frac{du}{dy} = \frac{u_\tau}{\kappa y} \qquad \mu_t = \rho u_\tau \kappa y \tag{4.3.6}$$

L'hospital law and the laminar incompressible momentum equation were used for the case where the solution domain reached the wall.

5. Results and Discussion

5.1 Convergence Tests

Fig 5.1.1 shows Richardson extrapolation of the normalized displacement thickness ($Re_{\delta *}$) at the beginning of the transition from laminar to turbulent flow (the abscissa is the second power of grid cell size $h = \frac{1}{N}$) for the second order convergence of Arad et al. [5]. Second order convergence is clearly seen for fine mesh of 100-150 points but not for coarser grids of 80 points and less, where the numerical error exceeds 10 percent. Fourth order convergence shown in figure 5.1.2 is conserved in coarse grids of 20-30 points with an error of 4 percent. Even in the coarser mesh of 14-16 points the deviation from fourth order convergence is rather small, with an error of the order of 10 percent. The numerical error was estimated using Richardson extrapolation. The friction coefficient behaves in a very similar way. Pade et al. [8], with their fourth order solution of the Lees—Dorodnytzin transformed equations, and mixing length theory found that a 20 point mesh is required to obtain good accuracy. This shows a very high numerical efficiency of the present numerical scheme.

5.2 Comparison With Second Order Solutions

The high efficiency of the present scheme was tested by comparison of the present fourth and Arad et. al.'s [5] second order results for a flat plate boundary layer. The quantities shown are the stream-wise distributions of the friction coefficient C_f, the displacement thickness δ^*, and the momentum thickness Θ. The results of the fourth order solver, obtained on rather coarse grids (20 and 16 points in the lateral direction), where indistinguishable from the second-order-solver results, that were calculated on a mesh nearly ten times finer (150 points in the lateral direction).

Another characteristic of the flow are the profiles of the main variables across the boundary layer. The comparisons are made for the profiles of the main velocity component, the turbulence energy ($e = \frac{\sqrt{u'^2}}{U_\infty}$) and the product of the turbulence length scale and the turbulence energy (e*l). The results obtained are given in figures 5.2.1—5.2.3. 150 point grid was used for the second order case, and a 20 point grid in the fourth order case. The profiles for the two meshes are in a good agreement.

5.3 Efficiency Measurements

It has been shown that the fourth order solution yields accurate results on much coarser grids than the second order solution. This is shown again in figure 5.3.1, showing the errors of the second and fourth order schemes. The "exact" solution (of a typical parameter, like the transition location) is obtained using Richardson extrapolation to zero mesh size. The approximation error, defined as

$$\epsilon = f_{h_0} - f_{h_N}$$

can be plotted against the mesh size For coarse grids the fourth order solver is about five times more accurate. For the finer grids, its accuracy is two orders of magnitude better than that of the second order solver.

The computational efficiency depends not only on the accuracy but also on the numerical load. Indeed the additional complexity of the fourth order solution tends to increase the computer time required. The necessity to compute explicitly the first derivative of the diffusion coefficient (see ch. 4.3) aggravated the situation even more. Hence, it is required to check the efficiency of the higher order solution. The CPU time required for the various solvers, per step, is plotted in figure 5.3.2 versus the number of grid points. It reveals that one fourth order step requires, approximately, twice the typical time necessary for a second order step. On the other hand the memory requirement is reduced by an order of magnitude, while the CPU time is only doubled. The total efficiency of the new solver is well displayed in figure 5.3.3 showing the error versus the CPU time. The 20 points grid seems to be the most cost—effective mesh for the fourth order solver.

5.4 Comparison of Solution With Wall Functions and Solution up to The Wall

Results up to the wall, designated by SW are compared with results obtained with wall functions designated here by WF. Once again the flat plat boundary layer was used as a test case. The development of the friction coefficient and integral thicknesses (displacement and momentum thicknesses) with x were in very good agreement for the two cases, and actually hardly distinguishable. The profiles are shown in figures 5.4.1-3. While the velocity profiles obtained with the two formulations are quite similar, small misfit appears in the turbulence energy profiles, in the inner surface. This disagreement seems to be caused by the empirical relation which was used as boundary condition for the turbulence energy (3.1.7). The solution up to the wall was performed here using 60 points mesh, while 14 point grid was used in the WF case. The resolution appears to be the same. This major saving in computational effort due to a combined use of wall functions and suitable coordinate stretching was discussed in ref [16]. In that work, 6 points grid with appropriate stretching, gave the same accuracy as 60 points, regularly spaced mesh (The 1D boundary layer was the test case, and numerical solutions were compared with the analytical solution). It was also found that within a stability margin, the sensitivity to the stretching parameter is weak.

5.5 Test of The Influence of Boundary Layer Thickness Calculation

The method for approximating the boundary layer thickness was described in section 3.3. This approach is

supposed to be insensitive to grid-fineness, unlike the conventional Patankar and Spalding [9] method. The values calculated by the latter method (designated as *method 1*) using a fine and a coarse grid, are compared in figure (5.5.1) with the result of the new method (*method 2*), using a coarse grid. As expected, while the mesh fineness had major effect on the first method, it had nearly no influence on the new method.

5.6 Validation of Results

To conclude the present representation, some comparison with experimental measurements is required. Test file 0612 of the 1982 Stanford conference [1] was used for that purpose (Flat plate boundary layer, $\frac{Re_x}{L} = 2.2 \cdot 10^6$, $U_\infty = 23m$). The conference standard comparisons are given in figures 5.6.1-3. Excellent agreement was achieved in the friction coefficient and velocity profile (in x=4.987m). The agreement of the H factor is not so good, but is in the same margin of accuracy as the other methods in that conference.

6. Conclusions

1. Wall functions can reduce the number of mesh points and the computational load very significantly. However, the formulae available for wall functions are not always sufficiently accurate.
2. Calculation of the boundary layer thickness using an integral technique improves the properties of the boundary layer thickness adaptive mesh.
3. The fourth order scheme is more accurate than the second order scheme, and its price performance is better.
4. An optimal generalized two equation turbulence model can be devised, with an optimal scale equation.
5. A numerical scheme for a turbulent boundary layer differs in some important aspects from that of a laminar boundary layer.

7. References

1. S.J. Kline, B.J. Cantwell and G.M. Lilley (Ed.), "Complex Turbulent Flows", Thermo-sciences Division, Mechanical Engineering Department, Stanford University, 1982.
2. Jones W. P. and Launder B. E., "The Prediction of Laminarization of A Two-Equation Model of Turbulence", Int. J. of Heat and Mass Trans., Vol. 15, 1972, p. 301
3. Mansour M., Kim J. and Moin P., "Near Wall k-epsilon turbulence modeling", Turbulent Shear Flows Conference, Toulouse 1987
4. Wilcox D. C. and Rubesin W. M., "Progress in Turbulence Modeling for Complex Flow Fields Including Effects of Compressibility", NASA Tech. Paper 1517, 1980.
5. Arad E., Berger M., Israeli M. and Wolfshtein M., "Numerical Calculation of Transitional Boundary Layers", Int. J. of Num. Methods in Fluids, Vol. 2, pp. 1-23, 1982.
6. Lin A. and Wolfshtein M., "Tensorial Volume of Turbulence", Phys. of Fluids, Vol. 23, No. 3, 1980, pp.644-646.
7. Zeierman S. and Wolfshtein M., "Turbulent Time Scale for Turbulent Flow Calculations", AIAA J., Vol. 24, No. 10, 1986, pp.1606-1610.
8. Pade O., Postan A., Anshelovitz D. and Wolfshtein M., "Incorporation of Boundary Conditions in Boundary Layer Fourth Order Solutions With Stretching in The Normal Direction", Proc. of Int. Conf. on Num. Methods in Laminar and Turbulent Flows, Seattle, Pineridge Press, Swansea, U.K., Aug. 1983.
9. Patankar S. V. and Spalding D. B., "Heat and Mass Transfer in Boundary Layers", 2nd. Ed., Int. Textbook Co. Ltd., London 1970.
10. Cebeci T., and Smith A. M. O., "Analysis of Turbulent Boundary Layers", Academic Press, New York, 1974.
11. Keller H. B. and Cebeci T., "Accurate Numerical Methods for Boundary Layers Flow—II. Two Dimensional Turbulent Flows", AIAA J., Vol. 10, p.1193, 1972.
12. Postan A., Pade O., Anshelovitz D. and Wolfshtein M., "Accurate Solutions for Laminar and Turbulent Boundary Layers at Very large Pressure Gradients", in Numerical Method in Laminar and turbulent Flows (Taylor C. and Schrefler B. A. Ed.), Pineridge Press, 1981.
13. Swartz B. K., "The Construction of Finite Difference Analogs of Some Finite Element Schemes", in Mathematical Aspects of Finite Elements in Partial Differential Equations, (C. DeBoor Ed.), pp.279-312, Academic Press, New York, 1974.
14. Ciment M., Leventhal S. H., Weinberg B. C., "The Operator Compact Implicit Method of Parabolic Equations", J. of Comp. Phys., Vol 28, pp 135-166, 1978.
15. Berger A. E., Solomon J. M., Ciment M., Leventhal S. H. and Weinberg B. C., "Generalized OCI Schemes for Boundary Layer Problems", Math. of Comp., Vol. 35, No. 151, pp 695-731, 1980.
16. Arad E. and Wolfshtein M., "Gradient Boundary Conditions for Turbulent Flows", Int. Symp. on Comp. Fluid Dyn., Sydney, Aust., 1987.
17. Israeli M. and Livne A., "Development of a "Super Stable" Scheme of Second Order in The Flow Direction, and Fourth Order in The Cross-Flow Direction, for Boundary Layers Equations", Aerodynamic Laboratory Rep. No. 160-073, Technion, Israel, 1977 (in Hebrew).

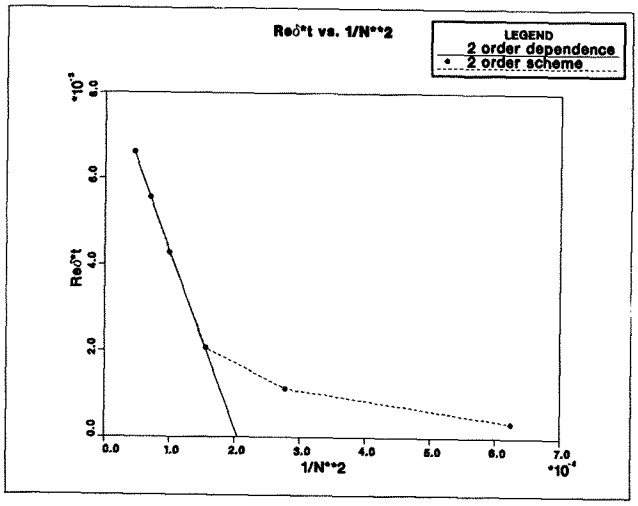

Figure 5.1.1: Richardson Extr. of $Re_{\delta * t}$ vs. h^2 for 2 order solver

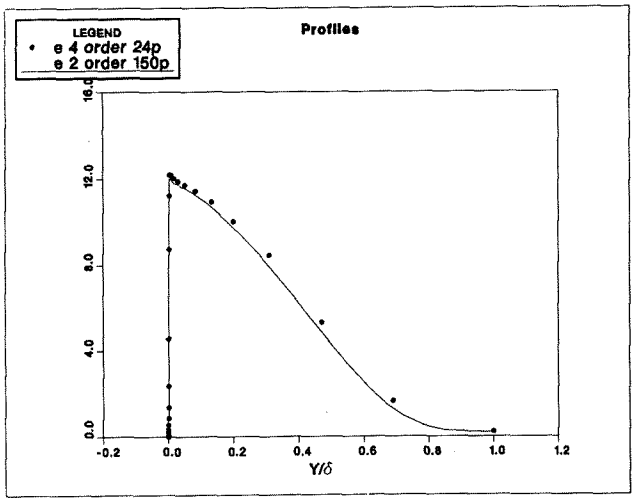

Figure 5.2.2: Turbulence energy profiles in a turbulent boundary layer

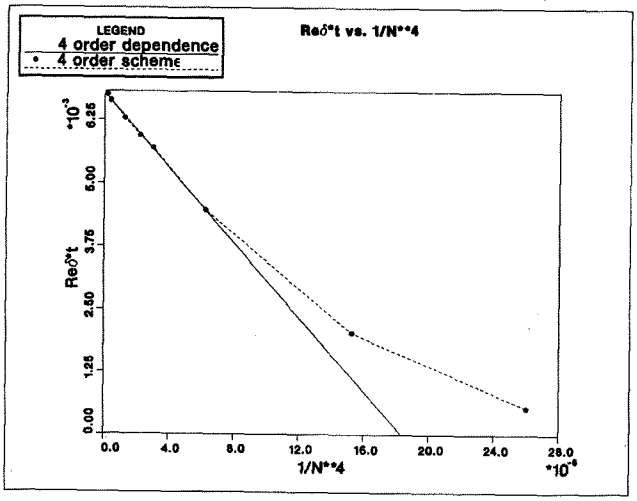

Figure 5.1.2: Richardson Extr. of $Re_{\delta * t}$ vs. h^4 for 4 order solver

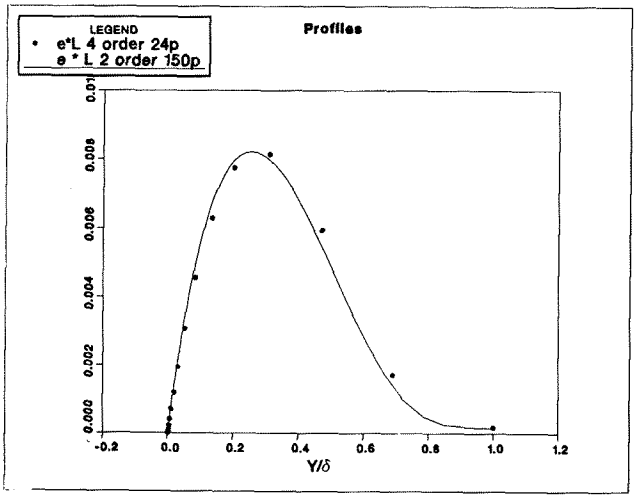

Figure 5.2.3: e*l profiles in a turbulent boundary layer

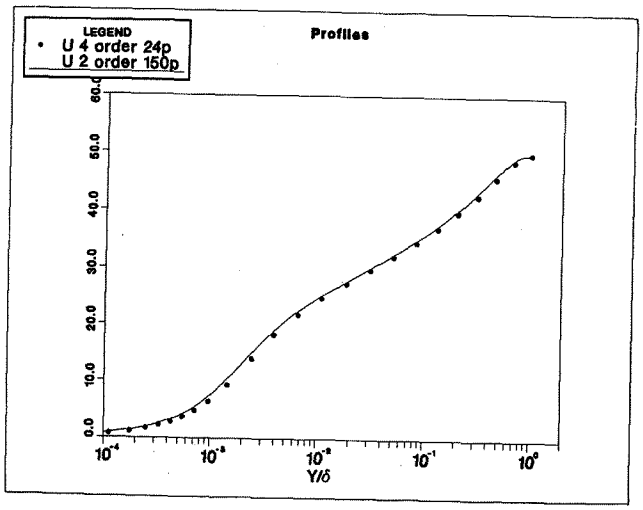

Figure 5.2.1: Velocity profiles in a turbulent boundary layer

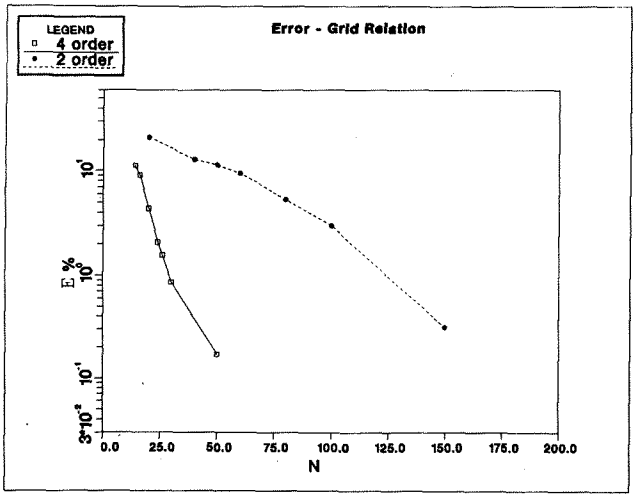

Figure 5.3.1: Computational error of the two solvers

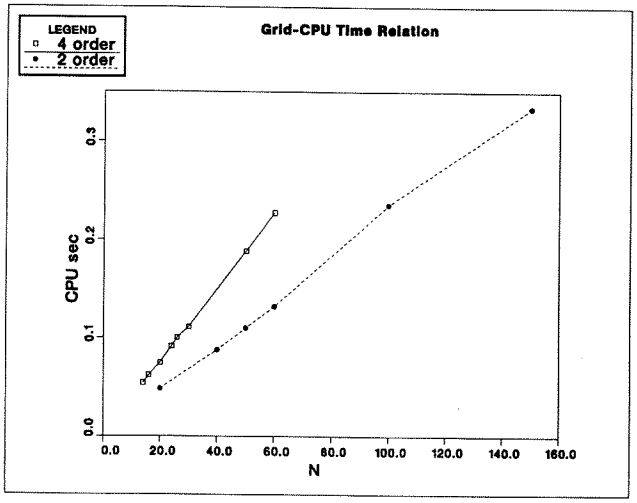

Figure 5.3.2: CPU time requirements of the two solvers

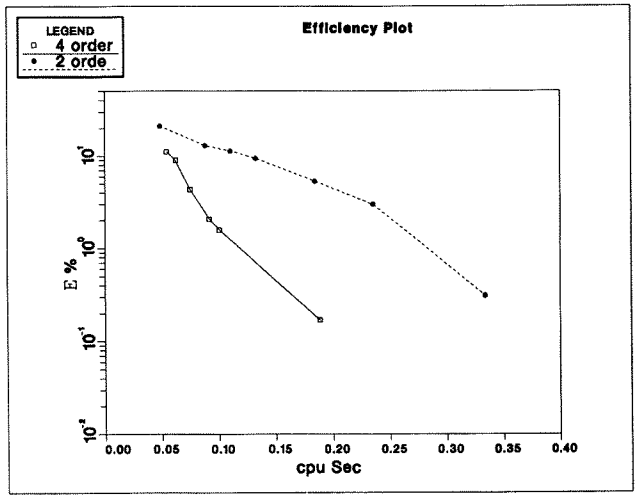

Figure 5.3.3: Efficiency plot: Computational error vs. CPU time for the two solvers

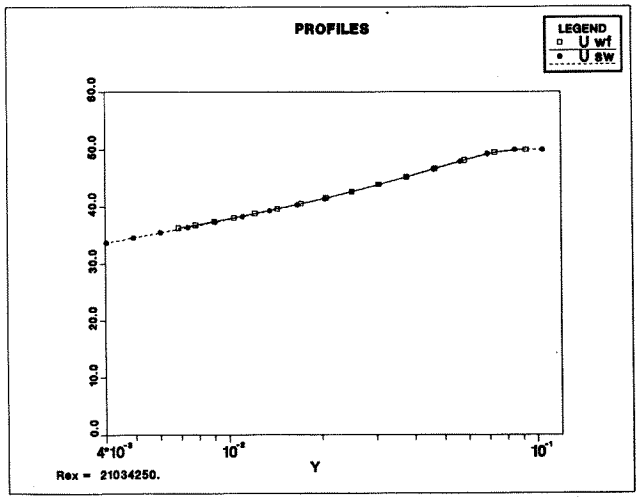

Figure 5.4.1: Velocity profiles calculated with and without wall functions

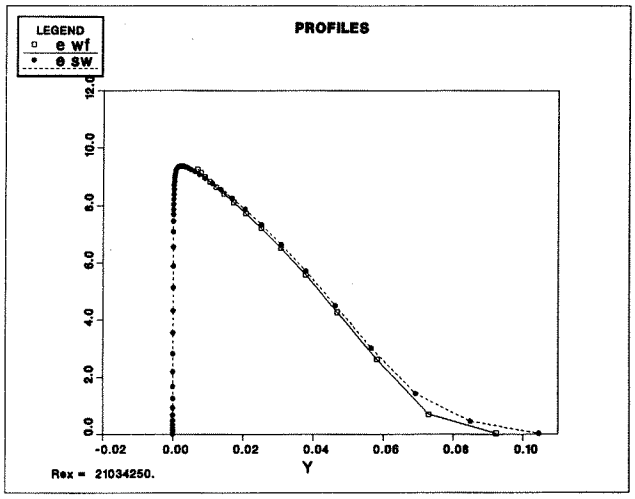

Figure 5.4.2: Turbulence energy profiles calculated with and without wall functions

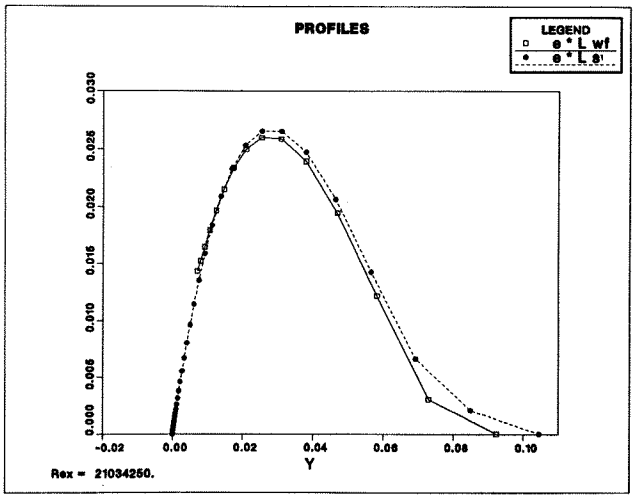

Figure 5.4.3: e*l profiles calculated with and without wall functions

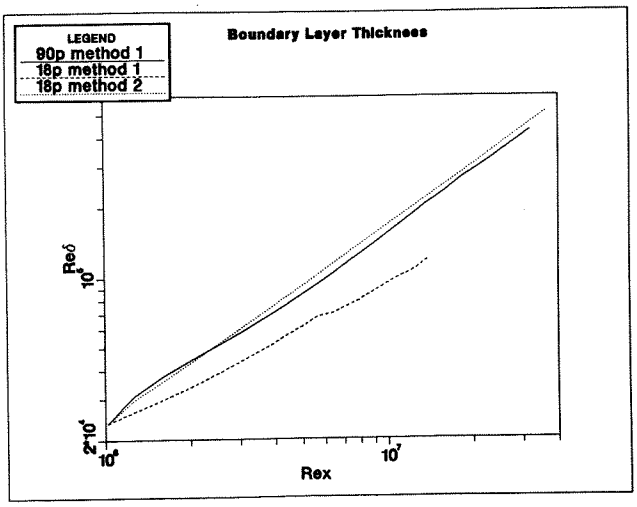

Figure 5.5.1: The influence of mesh-fineness on boundary layer thickness approximation

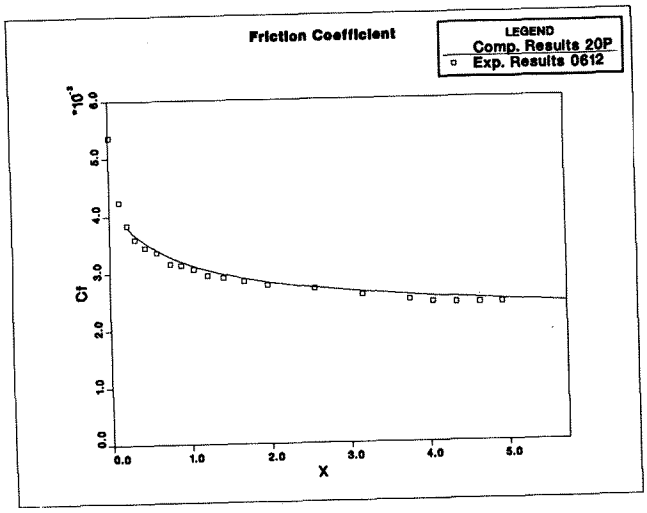

Figure 5.6.1: Comparison of computed flat plate friction coefficient with experimental measurements

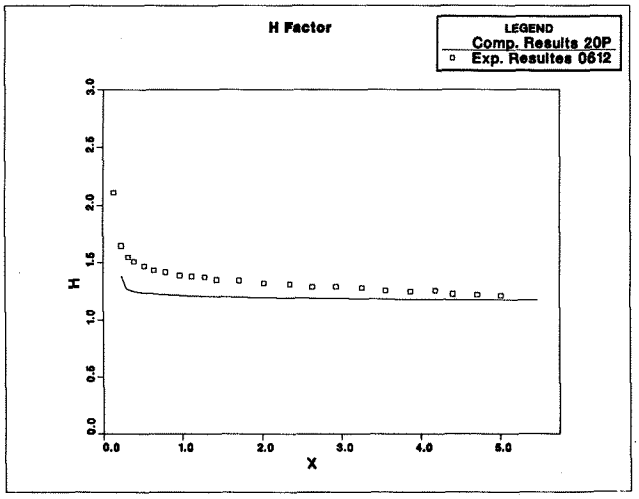

Figure 5.6.2: Comparison of computed flat plate H factor with experimental measurements

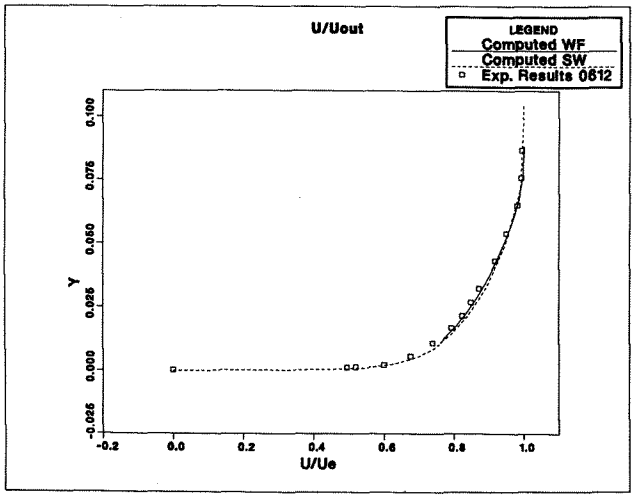

Figure 5.6.3: Comparison of computed velocity profile with experimental measurements (x=4.987m)